Tortuosity estimate through paramagnetic gas diffusion in rock saturated with two fluids using T_2 (z, t) low-field NMR

Igor Shikhov [1] *and Christoph H. Arns* [1]

[1] School of Petroleum Engineering, University of New South Wales, Australia

Corresponding author: Christoph H. Arns, School of Petroleum Engineering, University of New South Wales Sydney, e-mail: c.arns@unsw.edu.au

(received 28.02.2017, accepted 29.06.2017)

Abstract

Petrophysical interpretation of ^{1}H NMR relaxation responses from saturated rocks is complicated by paramagnetic species present in fluids. Oxygen dissolved in liquids is one common example. Dipolar interactions of oxygen's unpaired electron spins with the magnetic moment of fluid nuclei provide a strong relaxation mechanism known as paramagnetic relaxation enhancement (PRE). As a result even low concentrations of dioxygen in its common triplet ground state significantly shorten longitudinal and transverse relaxation times of host fluids. This effect may be employed similarly to any standard tracer technique to study pore connectivity in porous media by detecting a change of oxygen concentration due to diffusion resolved in time and space. Since relaxation enhancement effect is likely stronger in non-wetting phase than in wetting one (where surface relaxation process dominates) this difference can be utilized to study wettability in immiscible multiphase systems.

We use a relaxation time contrast between air-saturated and oxygen-free fluids to evaluate oxygen concentration change within two fluid phases saturating rock, to estimate time required to establish equilibrium concentration and to calculate a mutual diffusion coefficient of oxygen. A spatially- and time-resolved $T_2(z,t)$ experiment provides the time-dependent oxygen concentration change along the fully- and partially-saturated carbonate core plug exposed to air saturated oil at its inlet. We derive an effective mutual diffusion coefficient of oxygen and accordingly a tortuosity estimate as a function of position along the core and rock saturation.

The spatially resolved oxygen diffusion-based tortuosity is compared to simulated conductivity-based tortuosity. The latter is calculated on a high-resolution micro-tomographic image of Mount Gambier limestone by solving the Laplace equation for conductivity.

Keywords

paramagnetic relaxation enhancement, oxygen effective diffusion, tortuosity, wettability

1. Introduction

1.1 Paramagnetic relaxation enhancement (PRE)

Dissolved dioxygen O_2 present in fluids shortens their longitudinal and transverse relaxation times due to NMR paramagnetic enhancement (PRE) [1,2]. This may affect petrophysical interpretation of NMR responses from saturated rocks [3]. The effect arises due to the unpaired electron spin present in certain species, like O_2, Mn^{2+}, Fe^{2+}, Fe^{3+}, Gd^{3+}, etc. Paramagnetic electron – nuclear interactions have a much longer range than spin-nuclear spin interactions (proportional to $\langle r^{-6} \rangle$, where r is the distance between the unpaired electron and the proton of interest). Accordingly, the PRE effect is very large relative to interactions between protons owing to the large magnetic moment of an unpaired electron permitting interaction distances up to 35 Å [4] ($\gamma_e \sim 660\ \gamma_p$, where γ_e and γ_p are the gyromagnetic ratios of electron and proton respectively).

We study a system which consists of water and refined oil saturating a carbonate rock core, exposed to air saturated oil at one inlet. The effect of chemical interaction of fresh water with the solid constituents of the rock here is neglected, which may be an inappropriate approximation. To evaluate the influence of released ions on NMR relaxation, we measured the change of pH of an aqueous solution saturating the rock over time. From XRF elemental oxides measurements we know that Mount Gambier carbonate is completely free from manganese, and copper. The majority of ions released from the solid phase into the water are diamagnetic Ca^{2+} ions with addition of minor fractions of Mg^{2+} and Na^{+} ions which are also diamagnetic. However, it was detected that this rock has substantial iron content (0.19 wt% Fe_2O_3). We may assume that a certain amount of Fe^{2+} and Fe^{3+} paramagnetic ions (4 and 5 unpaired electrons in the ground state respectively) can be released over time. The pH of water saturating this carbonate sample becomes weakly alkaline over time until reaching pH=8.3. However, this has no observable effect on the bulk relaxation time of the solution, which suggests the effective binding of metal ions by carbonate/bicarbonate.

We can estimate transport properties of a porous medium by observing the dynamics of oxygen concentration change along the core. The concentration of dissolved oxygen (a normalized fraction), f_{O_2} in the bulk fluid can be calculated using relaxation time $T_{2,\text{pure}}$ of a system at oxygen-free state and observed relaxation time $T_{2,\text{obs}}$ of oxygen enriched system using following equations, [1,5]:

$$\frac{1}{T_{2,obs}} = \frac{1}{T_{2,pure}} + \frac{f_{oxy}}{T_{2,oxy}}, \text{ and } \frac{1}{T_{2,oxy}} = \frac{a\, n_{oxy} \gamma_p^2 \gamma_e^2 \eta}{T_K}\ , \tag{1}$$

where n_{oxy} – concentration of oxygen in solution. In the case of saturated rock the first term of the left-side equation contains two relaxation time terms: bulk fluid $1/T_{2,B}$ and surface relaxation rate $1/T_{2,S}$. Transport and evolution of oxygen concentration have been routinely studied in medicine, chemical and bioengineering, soil sciences etc. These studies typically consider diffusion of oxygen in a single phase saturating the porous medium (e.g. soil or rock) [6]. High-field NMR relaxometry was employed to determine the average effective diffusion and tortuosity in a water-saturated sand pack using 2,2,6,6-tetramethylpiperidine-1-oxyl tracer [7]. Heterogeneous systems like sedimentary rocks can be studied by using spatially-resolved NMR techniques. For instance, 1D-resolved profiling and relaxation low-field NMR techniques are particularly popular in characterization of rock cores, providing estimates of valuable petrophysical properties [8]. We expand application of NMR profiling techniques to study tortuosity and fluid continuity in heterogeneous carbonate rock saturated with immiscible fluids. Spatially and temporary resolved concentration of a paramagnetic tracer (oxygen O_2) in each of two fluids enabling estimation of local diffusion coefficients, $D_{O_2}(z)$, and diffusive rock tortuosity, $\tau_d(z)$. The similarity between diffusion and electrical conductivity is long known [9]. Here we tested the approach experimentally targeting the oil phase. We compare tortuosity calculated from effective diffusion $\tau_d(z)$

to numerically simulated conductivity $\tau_e(z)$ obtained by solving the Laplace equation on a micro-tomographic image of Mount Gambier limestone capturing a full-size core plug of 5.08 *cm* in length and 2.54 *cm* in diameter (the same core is used in NMR experiments).

1.2 O_2 concentration from NMR relaxation

Consider a cylindrical rock core partially saturated with oxygen-free water and oil with boundary (inlet) exposed to oil saturated with air and all other boundaries closed. Air diffuses towards lower concentration along the core following two pathways or their combination: (1) along the connected path of oil; (2) diffuses across the interface of isolated oil patches into water and back into the next isolated oil patch (which is likely a slow mechanism). The spatially-resolved effective diffusion coefficient can be obtained by solving 1D concentration-equation (weighted by local porosity) [10]:

$$\frac{\partial C(z,t)}{\partial t} = D_e(z)\,\frac{\partial^2 C(z,t)}{\partial z^2}, \tag{2}$$

where $C(z,t)$ is concentration of oxygen in the solution, t is time and D_e is the mutual diffusion coefficient of a tracer in the fluid. Boundary conditions are constant concentration at inlet $C(0,t) = C_0$ and open at the outlet with side boundaries closed. For two fluids an additional boundary condition is set at the fluids interface proportional to the relative solubility gradient on both sides of the interface.

The solubility of oxygen in water in equilibrium with air is 8.5 *mg/L* at 25°*C*, while solubility in *n*-paraffins is almost an order of magnitude higher, 71 *mg/L* at 25°*C* for *n*-decane. The mutual diffusion coefficient of oxygen in *n*-alkanes is also much higher than one in water, $5.5\cdot10^{-5}$ cm^2/s comparing to $2.2\cdot10^{-5}$ cm^2/s. The analytical solution to Eqn. (2) with relevant boundary and initial conditions is used to derive the effective oxygen diffusion coefficient from experimental relaxation data:

$$C(z,t) = C_0\left(1 - erf\left\{\frac{z}{\sqrt{4Dt}}\right\}\right). \tag{3}$$

2. Methods and materials

2.1 Relaxation contrast due to PRE

Experimental measurements and numerical simulations were performed on Mount Gambier outcrop carbonate from South Australia. Mount Gambier limestone exhibits remarkably high porosity, φ to brine is about 52% and permeability to brine 4.4 μm^2. The majority of pore space is associated with very large pores (82% of effective porosity is resolved at 10.95 *μm/voxel* resolution). Fig.1 [a, b] shows the effect of dissolved oxygen on NMR T_2 relaxation for the case of fully decane saturated core.

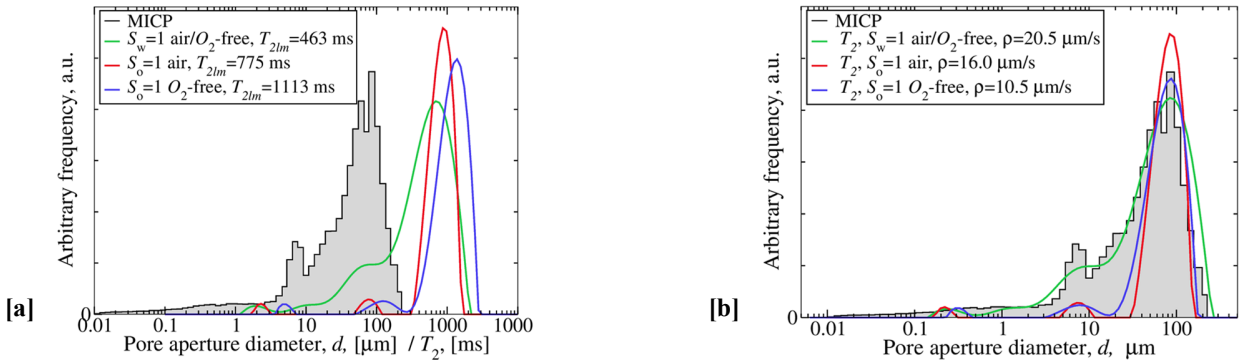

Figure 1: [a] Comparison of experimental T_2 distributions of a core fully saturated with water or oil in equilibrium with air / oxygen-free states. [b] Shift of T_2 responses to match mode MICP values at fully water and fully oil saturation states (air-saturated and O_2-free). The effect is expressed through apparent relaxivity ρ_2.

Matching modes of MICP and T_2 distributions in air-saturated and oxygen-free states requires application of 60% lower effective relaxivity ρ_2 for O_2-free oil case (10.5 *μm/s* comparing to 16.0 *μm/s*). The impact on mean relaxation time is very strong when dealing with decane as a representation of light oil, Fig.1 [a]. Interestingly, no difference between T_2 distributions obtained on fully water saturated Mount Gambier core was observed irrespectively whether or not water was deoxygenated, while bulk water $T_{2,B}$ shows an easily detectable difference (with $T_{2,B}$ of 3.2 *sec* and 2.5 *sec* respectively). This implies that such measurements are inherently sensitive to wettability conditions or certainly tell if rock is water-wet when surface relaxation dominates.

Table 1. Relaxation contrast of air-saturated and oxygen-free Mount Gambier cores.

Sample	+air, T_2 [*ms*]	O_2-free, T_2 [*ms*]	Ratio, O_2-free/air
bulk water	2470	3220	1.30
MtG, S_w=100%	463	463	1.00
bulk *n*-decane	1250	2850	2.28
MtG, S_o=100%	775	1113	1.44
MtG, S_o=51%+D_2O	1077	1983	1.84

Using a time-series of CPMG measurements we experimentally evaluated the impediment of water-oil interface on oxygen mass transfer. The samples were 20 *mL* vials filled with nitrogen-saturated water in one instance exposed to air and in another sealed with air-saturated decane. While the geometry of such systems matters, some estimates can be obtained about time scales. Expectedly, oxygen diffuses from decane into water at significantly reduced rate (it takes 6 to 8 times longer to reach equilibrium with air, 20 vs. 3 hours for the system of core plug size).

2.2 $T_2(z, t)$ relaxation experiment

We employed a frequency-encode (i.e. constant gradient) CPMG-T_2 experiment repeated with regular time intervals (e.g. every 6 ½ *min*) to obtain temporary and 1D spatially resolved relaxation data. In our experiments SNR was balanced with the need for quick acquisition time (one $T_2(z,t)$ data point was averaged over 1 *min*), therefore signal-to-noise was rather moderate: 83 for bulk sample, 54 for fully saturated core and 28 for partially saturated core. We used 4-step phase cycling. One-dimensional constant field gradient is a linear variation of the magnetic field strength with respect to one direction: $B(z) = B_0 + z\ G_z$. Thus, for the static field B_0 which set the Larmor resonant frequency ω_o, the presence of such a gradient G_z the standard CPMG experiment resulted in a signal which consists of a sequence of superimposed echoes with different frequencies. The spectrum of each echo can be obtained via Fourier transform. This procedure is called frequency encoding and causes the resonance frequency to be proportional to the position of the spins. This is illustrated by the following equalities, assuming a gradient direction aligned to *z*-axis:

$$\omega_0(z) = \gamma B(z) = \gamma(B_0 + zG_z) = \ \omega_0 + \gamma z G_z \ . \tag{4}$$

The observed time-dependent signal originated from the contribution of all cites having different frequencies ω is given by the following integral:

$$\frac{M(t)}{M(0)} = \int f(\omega)\, e^{i\omega t} d\omega \ . \tag{5}$$

The frequency spectrum can be obtained via Fourier transform of Eqn.(5):

$$f(\omega) = \ \int \frac{M(t)}{M(0)}\, f(\omega) e^{-i\omega t} dt \ . \tag{6}$$

Taking into account Eqn. (4), concept of k-vector, $k = \gamma g t / 2\pi$ and noting that $dt = (2\pi/\gamma g)dk$ the integral equation Eqn.(6) can be re-arranged to change variables as follows:

$$f(z) = \int h(k) e^{-i2\pi kz} dk \,, \tag{7}$$

where $h(k) = M(k)/M(0)$ is a normalized magnetization as a function of k. Data acquired experimentally are in a discrete form. Correspondingly, a discrete form of Fourier transform (DFT) is applied. For discrete position-dependent intensity distribution function $f(z_i)$ the integral Eqn.(7) becomes

$$f(z_i) = \sum_{j=0}^{N} h(k_j) e^{-i2\pi k_j z_i} \,. \tag{8}$$

Fig. 2 shows the pulse sequence diagram of a $T_2(z,t)$ experiment. It consists of a CPMG echo-train with constant gradient applied to obtain spatial domain, repeated at a regular time interval T_R. The echo time TE is selected to be sufficiently long to collect spectra in frequency domain within each echo time interval (here TE=3.2 ms). The obtained series of echoes then was processed using 2D FFT along the frequency domain. Resultant $M(z,t)$ decays were inverted into $T_2(z,t)$ using a series of 1D inverse Laplace Transforms (regularized NNLS algorithm [11]).

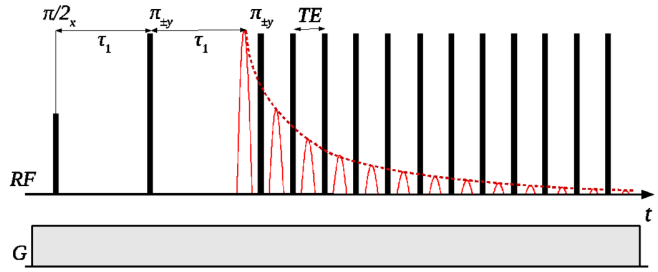

Figure 2: A pulse sequence diagram of a T_2 (z,t) experiment, where the CPMG echo-train in the presence of a constant gradient was repeated at a regular time interval.

2.3 Conductivity simulation

We calculated electrical tortuosity $\tau_e = \varphi\, c_e/c_o$ in a non-wetting (oil) phase in a rock by simulating the conductivity as a function of local saturation. The experimental measurements of conductivity in oil phase would be complicated and have not been attempted here. The series of fluid saturation states was simulated using capillary drainage transform on rock voxelized representation – an idealized numerical drainage experiment [12]. Electrical conduction is governed by Laplace equation since in steady state electric field $\boldsymbol{E}$ the potential φ obeys $\nabla^2 \varphi = 0$. Using no-flux boundary at the solid surface and specified macroscopic potential gradient the problem is solved using a conjugate gradient technique to evaluate the field. Further details can be found in [13,14].

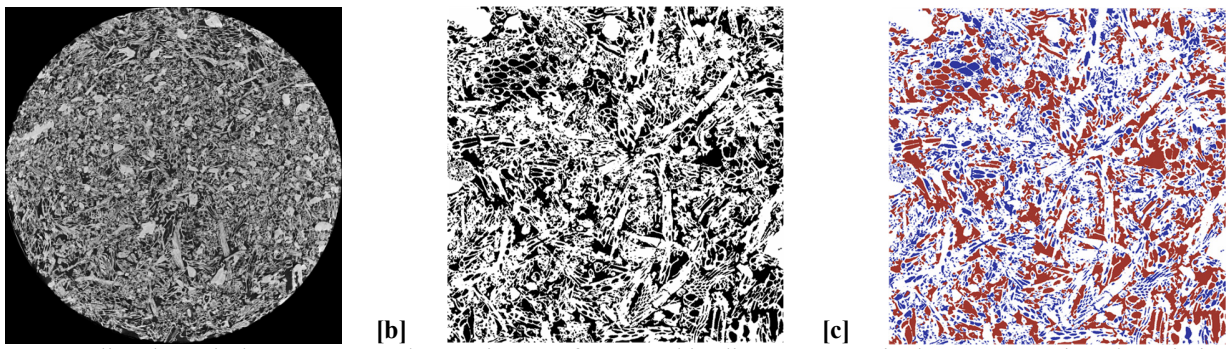

Figure 3: [a] Slice through the reconstructed µ-CT image of Mt Gambier limestone acquired at 10.95 *µm/voxel* resolution (FOV 2160 x 2160 voxel). [b] Subsection of two-phase solid-solid segmented image (1440 x 1440 voxel). [c] Slice through the image once capillary drainage transformation (CDT) is applied. It enables to mimic distribution of fluids in assumption of perfect water wetting conditions, S_o = 48.9%.

3. Results and discussion

The relaxation contrast between bulk fluids and saturated Mount Gambier rock offered by oxygen is given in Table 2. Note, there is no difference in $T_{2,LM}$ in a fully water saturated sample because surface relaxation is a dom*τ*inating process. Decane can carry eight times more oxygen than water and offers four times greater bulk relaxation time contrast between oxygen-free and air-saturated fluid (in our experiments oxygen is always a fraction of that gas in the air, i.e. 0.209). Expectedly, in a partially saturated rock, where the aqueous phase is replaced with deuterium oxide D_2O, the difference between oxygen-free and air-saturated states is higher than in fully decane saturated rock, but less than in bulk decane sample. This evidences partially oil wetting conditions.

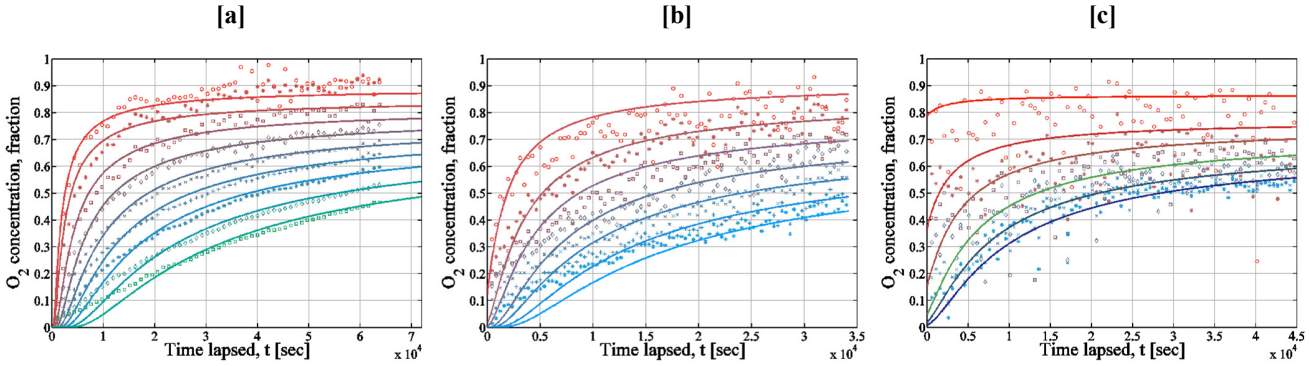

Figure 4: Evolution of oxygen concentration along the sample length, $O_2(z,\ t)$ derived from $T_2(z,\ t)$ experiments for the following cases: [a] the first nine 3-*mm* slabs of a bulk *n*-decane sample (the sponge soaked with *n*-decane was used to avoid convection); [b] the first seven slabs of a 2-*in* long x 1-*in* diameter Mount Gambier carbonate sample fully saturated with *n*-decane; [c] the first six slabs of that Mount Gambier sample partially saturated with D_2O and *n*-decane, S_o=51%.

Fig.4 [a,b,c] shows time-evolution of oxygen concentration along the core (in 3-*mm* slabs) calculated from $T_2\,(z,t)$ experiments. Initially, the core was fully saturated with deoxygenated *n*-decane, following exposure of the inlet to bulk decane equilibrated with air. Fitting data to analytical solution results in the following oxygen effective diffusion coefficients: (1) in bulk decane $D_{e,O2} = 6.9{\cdot}10^{-5}$ cm^2/s; (2) in Mt Gambier at S_o=100% $D_{e,O2} = 6.1{\cdot}10^{-5}$ cm^2/s; (3) in Mt Gambier at S_o=51% $D_{e,O2} = 3.7{\cdot}10^{-5}$ cm^2/s. Here we define D_e-based tortuosity as $\tau_d = \varphi\ D_e/D_o$, i.e. increase in pathway due structure complexity corresponds to decrease in tortuosity τ, though, inverse definitions are also common.

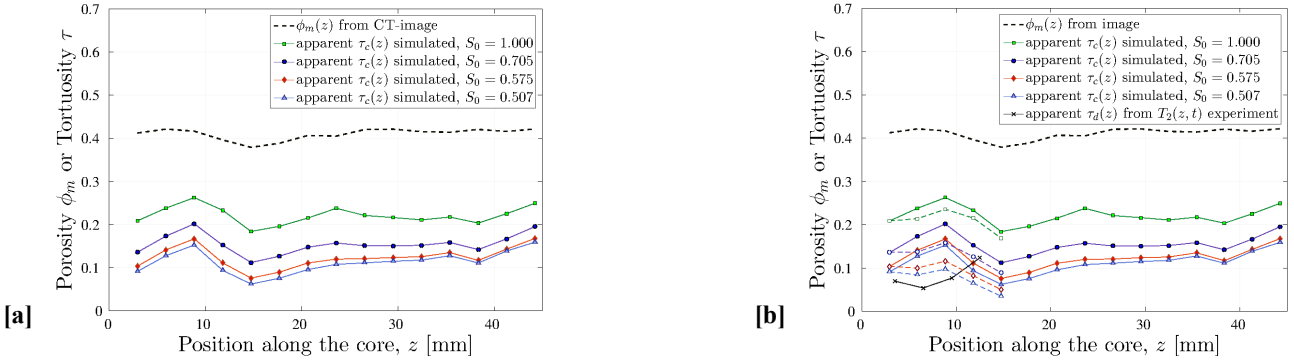

Figure 5: [a] Macro-porosity along the micro-CT image of Mount Gambier and the apparent tortuosity values of non-wetting phase calculated at various points along the image at four different saturations. The distance along the core is counted from inlet face of a core exposed to oxygen-saturated decane. [b] Four dashed lines in interval 3 to 15 *mm* correspond to tortuosity of each 3-*mm* slab extracted from apparent (cumulative) tortuosity values. The black solid line is tortuosity calculated from experimental NMR relaxation data.

Another tortuosity estimate is obtained by solving Laplace equation for conductivity on a voxelized image, $\tau_e = \varphi\ c_e/c_o$ assuming perfectly water-wet conditions, Fig.5 [a]. Tortuosity estimate based on oxygen diffusion is expectedly higher ($\tau_d < \tau_e$) than conductivity since some transport is possible between two phases, Fig.5 [b]. It reasonably well captures the change of tortuosity due to saturation decrease. Factors requiring further consideration include exposure of a core to atmosphere prior to NMR experiment; deoxygenating fluids by substitution of air with pure nitrogen, wettability conditions which may result in better oil connectivity and influence of microporosity which was not included in the numerical model.

Table 2. Tortuosity estimated from μ-CT image and $T_2(z,t)$ experiment.

sample	S_o = 1.0	S_o = 0.5	ratio
Core: $T_2(z,t)$, τ_d	0.451	0.248	1.82
Image: c, τ_e	0.186	0.054	3.44

4. Conclusions

We demonstrated that low-field NMR 1-D resolved relaxometry can be applied for quantitative characterization of multi-fluid systems saturating rocks by exploiting relaxation contrast offered by oxygen solubility and mobility in aqueous and oil phases. Interpretation of time- and spatially-resolved relaxation signal provides local effective diffusion coefficients of paramagnetic tracer weighed by local wetting conditions and phase continuity of a respective fluid. Potentially, the approach can provide information about spatial fluids distribution, diffusion tortuosity per phase and fluids interfacial area. The approach may be utilized to improve relative permeability estimates or to correct NMR signal for environmental effects, e.g. paramagnetic species in the drilling mud.

References

[1] G. Chiarotti, G. Cristiani, L. Giulotto, Il Nuovo Cimento 1(5) (1955) 863-873.
[2] I. Solomon, Phys. Rev. 99(2) (1955) 559-566.
[3] I. Shikhov, C.H. Arns, Appl. Magn. Reson. 47(12) (2016) 1391-1408.
[4] G.M. Clore, Biochem. Soc. Trans. 41(6) (2013) 1-23.
[5] A. Abragam, A. The principles of nuclear magnetism, Clarendon Press, Oxford, 1961.
[6] M. Aachib, M. Mbonimba, M. Aubertin, Water, Air & Soil Pollut. 156 (2004) 163-193.
[7] F. Furtado, P. Galvosas, F. Stalmach, U. Roland, J. Kärger, F.-D. Kopinke, Environ. Sci. & Technol. 45 (2011) 8866-8872.
[8] D.P. Green, J.R. Dick, J. Gardner, B.J. Balcom, B. Zhou, Comparison study of capillary pressure curves obtained using traditional centrifuge and magnetic resonanse imaging techniques, SCA2007-30, *Int. Symp. SCA*, *Calgary, Canada, 10-13.09.2007*.
[9] L.J. Klinkenberg, Bull. Geol. Soc. Am. 62 (1951) 559-562.
[10] J. Crank, The Mathematics of Diffusion, Clarendon Press, Oxford, 1975.
[11] C.L. Lawson and R.J. Hansen, Solving Least Squares Problems, Prentice-Hall, Englewood Cliffs, NJ, 1974.
[12] M. Hilpert, C.T. Miller, Adv. Water Res. 24 (2011) 243-255.
[13] P.M. Adler, C.G. Jacquin, J.-F. Thovert, Water Resources Res. 28(6) (1992) 1571-1576.
[14] C.H. Arns, M.A. Knackstedt, W.V. Pinczewski, W.B. Lindquist, Geophys. Res. Lett. 28(17) (2001) 3361-3364.